

The massive stellar content in NGC 604 and its evolutionary state.

Rosa M. González Delgado & Enrique Pérez

Instituto de Astrofísica de Andalucía (CSIC). Apdo. 3004, 18080 Granada, Spain

Accepted 1999. Received 1999; in original form 1999

ABSTRACT

This paper analyzes the integrated ultraviolet spectra taken with the *International Ultraviolet Explorer (IUE)* and optical ground-based spectra taken with the William Herschel Telescope (WHT) of the giant H II region NGC 604. These data are complemented with ultraviolet (WFPC2 through F170W) and H α (WFPC2 through F656N) images retrieved from the *Hubble Space Telescope (HST)* archive.

The ultraviolet resonance wind stellar lines, the nebular optical emission lines and the higher order terms of the Balmer series and HeI absorption lines detected in the spectra of NGC 604 are interpreted using evolutionary models optimized for young star forming regions. The evolutionary state and the massive stellar content of the region is derived in a self-consistent way.

The three techniques applied suggest that the central ionizing cluster in NGC 604 is very young, $\simeq 3$ Myr old, and that the stars in the cluster were formed in an instantaneous burst following a Salpeter ($\alpha=2.35$) or flatter ($\alpha=1.5$) initial mass function (IMF), having stars more massive than $80 M_{\odot}$. The stellar cluster is able to provide most of the ionizing photons needed to photoionize the whole nebula, and the wind power to form the central shell structure where the cluster core is located. The stellar cluster is affected by an extinction similar to the average extinction that affects the ionized gas. The estimated number of massive stars in the cluster is also in agreement with that derived from previous studies based on the detection of individual stars. The results that we present here support the use of these techniques for the interpretation of the integrated light of more distant star forming regions.

Key words: techniques: spectroscopic - galaxies: stellar clusters - ultraviolet: stars - ISM: H II regions - ISM: individual: NGC 604.

1 INTRODUCTION

Giant extragalactic H II regions (RH IIs) are amongst the brightest objects in galaxies. RH IIs have been studied extensively because they are the best indicators of the conditions that lead to massive star formation, and they show the cloud properties immediately after the moment when stars form. Equally important, they are favourable places where to measure the chemical abundances and star formation rates in galaxies, and hence can be used to trace the chemical and star formation history of the universe, when observed in galaxies at different redshift (Madau et al. 1996; Kobulnicky & Zaritsky 1999).

RH IIs are characterized to have a size larger than 100 pc and H α luminosity brighter than 10^{39} erg s $^{-1}$ (Kennicutt 1984). Therefore, the nebula requires an ionizing photon luminosity larger than 10^{51} s $^{-1}$; this is provided by a stellar cluster that contains more than 100 young massive

stars. These characteristics are very similar to those of starburst galaxies. However, they are less luminous than prototypical starbursts, and thus they are referred to as mini-starbursts (Walborn 1991). Like starbursts, RH IIs show a nebular emission-line spectrum at optical wavelengths, and an absorption-line spectrum at wavelengths shorter than the Balmer jump (Leitherer 1997; Rosa, Joubert & Benvenuti 1984). This spectral morphology reflects the fact that RH IIs are powered by massive stars. These stars emit photons with energies of tens of eV which are absorbed and re-emitted in their stellar winds, producing ultraviolet resonance transitions. However, the stellar wind is optically thin to most of the ultraviolet photons, that can travel tens of parsec from the star before they are absorbed and photoionize the surrounding interstellar medium. Subsequently, this ionized gas cools down via an emission spectrum. This spectral dichotomy picture allows to derive the stellar content and the evolutionary state of the cluster, through the anal-

ysis of the ultraviolet (e.g. Vacca et al. 1995; Leitherer et al. 1996), or the optical light (e.g. Cid Fernandes et al. 1992; García-Vargas & Díaz 1994; Stasińska & Leitherer 1996) using evolutionary synthesis and photoionization models. The two techniques have been applied to the prototypical starburst nucleus NGC 7714, giving similar results (González Delgado et al. 1999a).

However, around the Balmer jump the spectra of starbursts (González Delgado et al. 1998) and some H II regions (Terlevich et al. 1996) show the higher order terms of the Balmer series and He I lines in absorption, formed in the photospheres of massive stars. These stellar lines can be detected in absorption because the strength of the gaseous Balmer lines in emission decreases rapidly with decreasing wavelength, whereas the equivalent width of the stellar absorption lines is almost constant with wavelength (González Delgado, Leitherer & Heckman 1999b). Evolutionary synthesis models that predict the profiles of the higher order terms of the Balmer series and He I lines in absorption can also be used to estimate the evolutionary state of the stellar cluster in H II regions.

The second more luminous and brightest H II region in the Local Group of galaxies, after 30 Dor in the LMC, is NGC 604 in M 33. Its distance, 840 kpc (Freedman et al. 1991), allows detailed studies of the individual stars, and also to obtain integrated properties. Thus, NGC 604 is an excellent laboratory in which to explore questions about the effect of star formation, the slope and upper mass limit of the IMF, and to test the consistency between the three techniques described above, that allow to determine the stellar content and the evolutionary state of the ionizing stellar cluster from the spatially integrated ultraviolet and optical spectra of the H II region.

NGC 604 has been intensively studied in the past (e.g. Peimbert 1970; Israel & van der Kruit 1974; Smith 1975; Hawley & Grandi 1977; Kwitter & Aller 1981; Conti & Massey 1981; Rosa & D’Odorico 1982; Viallefond & Goss 1986). A precise determination of the chemical composition of the gas was made by Díaz et al. (1987); they give an oxygen abundance $12+\log(\text{O}/\text{H})=8.5$. VLA observations indicate that the gas is very tenuous (average electron density, $rms\ N_e$, between a few and $\sim 100\text{ cm}^{-3}$), and not very dusty, with a mean visual extinction $A_V \sim 0.5$ mag (Churchwell & Goss 1999). The morphology of the ionized gas is very complex, showing many filaments and shell structures that are expanding (e.g. Hippelein & Fried 1984; Rosa & Solf 1984; Clayton 1988; Sabalish et al. 1995; Muñoz-Tuñón et al. 1995; Yang et al. 1995; Medina Tanco et al. 1997). This morphology is a consequence of the violent star formation activity in NGC 604. *HST* imaging photometry has revealed that the stellar cluster is resolved into ~ 200 massive stars in an area of $\sim 10000\text{ pc}^2$ (Drissen, Moffat & Shara 1993; Hunter et al. 1996). Evidences that the stellar cluster is evolved come from the detection of Wolf-Rayet stars (Conti & Massey 1981; D’Odorico & Rosa 1981; Drissen, Moffat & Shara 1990, 1993), one supernova remnant (D’Odorico et al. 1980), and one candidate to red supergiant (Terlevich et al. 1996). The existence of these stars as members of the stellar cluster of NGC 604 suggests that the age of the region is in the range 3-5 Myr.

This paper presents spatially integrated ultraviolet and optical spectra of NGC 604. The goal is to derive the mas-

Figure 1. *HST*+WFPC2 (F170W) image of NGC 604 at ultraviolet wavelengths. The scale is $0.046\text{ arcsec pixel}^{-1}$, equivalent to $0.19\text{ pc pixel}^{-1}$. The rectangles mark the positions of the *IUE* apertures. North is up and East to the left.

Figure 2. *HST*+WFPC2 (F653N) image in the $\text{H}\alpha$ emission line (grayscale). The ultraviolet emission (F170W) is overlaid in white contours. The scale is $0.1\text{ arcsec pixel}^{-1}$. The lines indicate the slits of the ground-based optical spectroscopy. Note that the core of the cluster is within a nebular hole of 20 pc radius. North is up and East to the left.

sive stellar content and the evolutionary state of the ionizing cluster, by means of evolutionary synthesis and photoionization models applied to the ultraviolet resonance wind stellar lines, to the nebular emission lines and to the higher-order terms of the Balmer series and He I lines in absorption. The consistency between the results obtained with the three techniques, and the similarity with the results obtained from studies based on the detection of individual stars, strengthens the reliability and power of these techniques when they are applied to determine the stellar content of more distant star-forming regions. Section 2 presents the observations. Section 3 describes the photoionization models that fit the emission-line spectrum of the nebula. In section 4, the higher-order terms of the Balmer and He I lines in absorption are analyzed. Evolutionary synthesis models of the ultraviolet resonance wind stellar lines are in section 5. In section 6, the massive stellar content is derived. The summary and conclusions are in section 7.

2 OBSERVATIONS

2.1 *HST* images

NGC 604 has been intensively observed with the WFPC2 camera onboard the *HST*. For the purpose of this work, we have retrieved *HST* archive images at the ultraviolet (F170W filter) and optical $\text{H}\alpha$ (filter F656N) wavelengths. Two F170W exposures of 350 s each and two F656N exposures of 1000 s each were combined to produce one final ultraviolet (Fig. 1) and one $\text{H}\alpha$ image (Fig. 2). The nebula was centred in the PC camera, therefore the ionizing cluster is sampled at $0.046\text{ arcsec pixel}^{-1}$, corresponding to $0.19\text{ pc pixel}^{-1}$ (at a distance of 840 kpc, 1 arcsec corresponds to 4.1 pc). The ultraviolet emission is spread in the inner $20\times 20\text{ arcsec}$. The stellar density looks much lower than that observed in super star clusters. Surface brightness photometry indicates that 75 percent of the ultraviolet flux is produced by the core of the stellar cluster, that is contained within a central nebular hole of diameter $\sim 15\text{ arcsec}$; we shall refer to this as the centre of the nebula. The $\text{H}\alpha$ image shows many filaments and shell structures that extend out to $\sim 200\text{ pc}$ from the centre of the nebula. However, the brightest parts of the nebula trace almost a ring structure at a distance of 40 pc from the centre.

The total ultraviolet flux per unit wavelength in the F170W image is $1.9 \times 10^{-13}\text{ erg s}^{-1}\text{ cm}^{-2}\text{ \AA}^{-1}$. The $\text{H}\alpha$ flux is $4.0 \times 10^{-11}\text{ erg s}^{-1}\text{ cm}^{-2}$, in good agreement with the value measured by Churchwell & Goss (1999).

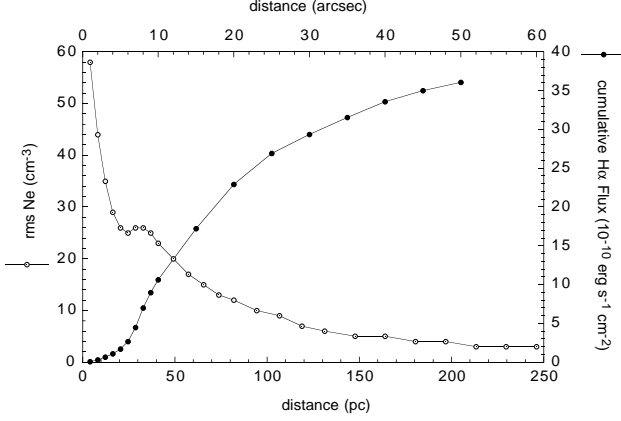


Figure 3. Cumulative H α flux (full dots) and the rms electron density (open dots) measured in the WFPC2 (F653N) image, using a circular aperture as a function of the distance to the center of the nebula.

We perform surface brightness photometry in the H α image using a circular aperture around the central cluster nebular hole. The cumulative flux is plotted in Fig. 3. This plot shows that 50, 75 and 90 percent of the total flux is contained in the inner 60, 100 and 140 pc radii^{*}, respectively. The H α flux distribution of NGC 604 has the characteristic features of a core-halo distribution, where the core can be quantitative and qualitatively explained by a thick shell structure. A detailed modelling of the geometry of NGC 604 will be presented elsewhere. The surface brightness weighted core radius of the region (following the method described in García-Vargas et al. 1997) is 80 pc.

The rms electron density is also estimated from the H α image as $(Q/\alpha_B V)^{1/2}$, where Q is the ionizing photon luminosity, α_B the total recombination coefficient of H, and V the volume of the ionized region. Fig. 3 also shows the rms N_e as a function of distance, that ranges from values between less than 100 cm⁻³ to a few cm⁻³, with rms N_e \sim 10 cm⁻³ at 100 pc from the center of the nebula.

2.2 Ultraviolet spectroscopy

NGC 604 has been observed with the *IUE* through the large aperture (9.5 \times 22 arcsec)[†] in low-dispersion mode, with either the SWP (1100–1900 Å) or the LWR (1900–3200 Å) cameras. The spectra were taken with the large aperture located at several different positions across the region. We have retrieved from the *IUE* Newly Extracted Spectra (INES, Rodríguez-Pascual et al. 1999; Cassatella et al. 2000) archive the spectra taken at the positions shown in Fig. 1 (see also Table 1). Several of the spectra were also retrieved in February 1997 from the *IUE* ULDA archive. When comparing the two different extractions of the same

^{*} Unless otherwise specified, distances refer to radial distances from the adopted centre of symmetry, as shown in Figs. 1 and 2.

[†] The precise form and size of the *IUE* large aperture is not known; we take a size of 22 \times 9.5 arcsec. The actual form is somewhat intermediate between the rectangle shown here and an enclosed ellipse.

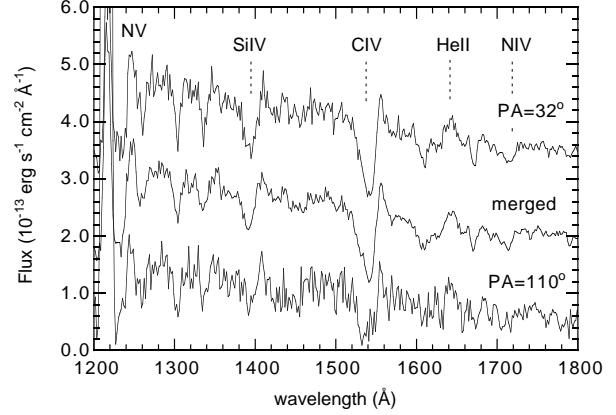


Figure 4. INES spectra of NGC 604 taken at PA=32°, and at PA=110°, and the average spectrum of those at PA=136°, 149° and 159°. The spectra are dereddened by $E(B - V) = 0.03$ using the MW Galactic extinction law. For the sake of clarity, the spectra at PA=32° and 110° are plotted after adding an artificial bias of $\pm 1.5 \times 10^{-13}$ erg s⁻¹ cm⁻² Å⁻¹, respectively. The most important wind resonance ultraviolet stellar lines are labelled. Other important absorption lines visible are formed in the intervening interstellar medium, and are of no concern to us here.

aperture spectrum, we noticed that the slope of the spectra were slightly steeper in the ULDA archive; both extractions have the same flux at 1500 Å but the ULDA extraction is 10 percent brighter at 1280 Å than the INES extraction. ULDA used a different extraction algorithm (IUESIPS) than INES, and their discrepancies are well documented (González-Riestra et al. 2000). INES represents the state of the art in the extraction of *IUE* spectra; so this is the data set that we use.

The flux at 1750 Å measured in the spectra SWP5688 (PA=149°) and SWP6638 (PA=110°) is 1.6×10^{-13} erg s⁻¹ cm⁻² Å⁻¹ and 1.3×10^{-13} erg s⁻¹ cm⁻² Å⁻¹, respectively. The sum total flux in these two apertures represents approximately the total ultraviolet flux emitted by the stellar cluster in NGC 604, and it amounts to 2.9×10^{-13} erg s⁻¹ cm⁻² Å⁻¹. This value is 45 percent larger than the total monochromatic flux measured in the F170W *HST* image ($F_{170} = 1.9 \times 10^{-13}$ erg s⁻¹ cm⁻² Å⁻¹). Fig. 4 shows the *IUE* spectra at PA=110° and at PA=32°, together with the average spectrum of those at PA=149°, 136° and 159°.

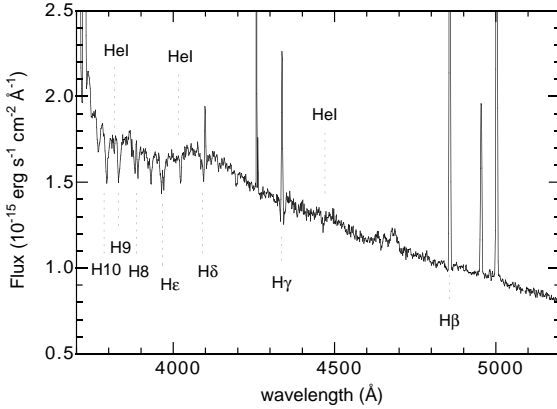
2.3 Optical spectroscopy

Optical spectra were obtained with the 4.2m William Herschel Telescope at the Observatorio del Roque de los Muchachos (La Palma), as part of the GEFÉ[‡] collaboration. The details of the observations and data reduction are in Terlevich et al. (1996). For the purpose of this work, we use the scanned spectra at PA=60° and at PA=120°, and the single long-slit spectrum at PA=131°. The scanned spectra

[‡] Grupo de Estudios de Formación Estelar, is an international collaboration formed to take advantage of the international time granted by the Comité Científico Internacional at the Observatories in the Canary Islands.

Table 1. Journal of Observations.

Telescope	Instrument	Filter or Grating	wavelength	P.A.	t_{exp} (s)	Image Name
<i>HST</i>	WFPC2	F170W	$\lambda_c=1750 \text{ \AA}$, $\Delta\lambda=545 \text{ \AA}$	–	2×350	U2C60B01T, U2C60B02T
<i>HST</i>	WFPC2	F656N	$\lambda_c=6564 \text{ \AA}$, $\Delta\lambda=21 \text{ \AA}$	–	2200	U2LX0301A
<i>IUE</i>	SWP		1100–1900 \AA	32°	12000	SWP19449
<i>IUE</i>	SWP		1100–1900 \AA	136°	15300	SWP19181
<i>IUE</i>	SWP		1100–1900 \AA	159°	6330	SWP7349
<i>IUE</i>	SWP		1100–1900 \AA	149°	6000	SWP5682
<i>IUE</i>	SWP		1100–1900 \AA	110°	4800	SWP6638
WHT	ISIS	G300B	3700–5500 \AA	131°	2×3600	
WHT	ISIS	G300B	3700–5500 \AA	60°	3600	
WHT	ISIS	G300B	3700–5500 \AA	120°	1800	
WHT	ISIS	G316R	7900–9700 \AA	60°	3600	
WHT	ISIS	G316R	7900–9700 \AA	120°	1800	

**Figure 5.** One-dimensional ground-based optical spectrum of NGC 604 obtained through a 1.2×4.6 arcsec aperture at the position where the continuum is maximum (see fig. 3b in Terlevich et al. 1996). The high-order terms of the Balmer series and He I $\lambda 4471$, He I $\lambda 4026$ and $\lambda 3819$ are labeled.

were centred at R.A. = $1^{\text{h}} 31^{\text{m}} 43^{\text{s}}$ and Dec = $30^\circ 31' 52''$, and they cover the core of the region by displacing a 1 arcsec wide longslit in steps of 1 arcsec and taking at each position a 1 minute exposure. The process is repeated until an area of $1.75' \times 0.18'$ (for the scan at PA = 120°) and $1.75' \times 0.23'$ (for the scan at PA = 60°) are covered (see Fig. 2). A one dimensional spectrum representative of the inner region of the nebula was obtained by merging the extractions that cover $11'' \times 60''$ (at PA = 120°) and $14'' \times 60''$ (at PA = 60°). At PA = 131° , a one-dimensional spectrum was extracted of length 4.6 arcsec, and centered at the position where the continuum is maximum (see fig. 3b in Terlevich et al. 1996). At this position the fraction of the stellar continuum with respect to the nebular emission lines is maximum, because it corresponds to the zone of the nebular hole. As previously noted by Terlevich et al. (1996), the spectrum shows the higher-order terms of the Balmer series and He I lines in absorption, and the continuum represents well the stellar light of the ionizing stellar cluster in NGC 604 (Fig. 5).

3 MODELLING THE NEBULAR EMISSION-LINES

The emission-line spectrum of an RH II depends on the radiation field from the ionizing stellar cluster, and on the density distribution and chemical composition of the gas. A photoionization code takes as input the spectral energy distribution of the cluster, and it solves the ionization-recombination and heating-cooling balances, to predict the ionization structure of the nebula, the electron density and the intensity of the emission lines. By comparing these output with observations, it is possible to obtain information about the ionizing stars and their evolutionary state.

The star formation law, age and massive stellar content of the stellar clusters can be constrained by comparing the observed emission line strengths with the predictions from the photoionization models, when the code uses as input the spectral energy distribution (SED) generated by a stellar evolutionary synthesis code. This technique has been used successfully to study the stellar content in starbursts and RH IIs (e.g. García-Vargas, Bressan & Díaz 1995a,b; García-Vargas et al. 1997; González Delgado et al. 1999a; Luridiana, Peimbert & Leitherer 1999; Stasińska & Schaerer 1999). Here, we fit the emission-line spectrum of NGC 604 using the photoionization code CLOUDY (version 90.04, Ferland 1997).

3.1 Input parameters

In order to predict the intensities of the emission lines, we fix the geometry of the nebula, the electron density and the chemical composition of the gas. We assume that the constant density gas is ionization bounded and spherically distributed around the ionizing cluster. The inner radius is 20 pc (as seen in the H α image), and the outer radius is determined by the ionization front. The results do not depend strongly on the inner radius if this changes by a factor 2 (e.g. Luridiana, Peimbert & Leitherer 1999). We assume that the gas occupies only a fraction of the sphere. Thus the filling factor, ϕ , is a free parameter with values of 10^{-1} , 5×10^{-2} , 10^{-2} , 10^{-3} and 10^{-4} . The change of filling factor is equivalent to changing the ionization parameter U , defined as $Q/(4\pi R N_e c)$; where Q is the ionizing photon luminosity, N_e the electron density, c the speed of light and R the distance

Table 2. Input parameters to CLOUDY.

12+log(O/H)	8.51
log (He/H)	-1.08
log (N/H)	-4.65
log (Ne/H)	-4.27
log (S/H)	-5.05
log Q	51.54 (s ⁻¹)
Inner Radius	20 pc
Ne	30, 100 cm ⁻³

of the gas to the ionizing source. For a spherical geometry, the average U is proportional to $(\phi^2 N_e Q)^{1/3}$.

The chemical abundances are fixed to those derived by Díaz et al. (1987). We scale the chemical composition of the gas to the value of the oxygen abundance, 12+log(O/H)=8.5, except the abundance of N, Ne, S and He, for which we take the values derived by Díaz et al. (1987; see Table 2). The electron density derived by Díaz et al. (1987) is of the order of 100 cm⁻³. Our measurements of the [S II]6717/6731 ratio indicate the low-density limit, with values below 100 cm⁻³ §. We have computed constant density models at two values of the electron density, 100 cm⁻³ and 30 cm⁻³. The latter value comes from the filling factor and an *rms* electron density of 10 cm⁻³, derived from the H α image. Also, an electron density of 30 cm⁻³ predicts a [S II]6717/6731 ratio which is in better agreement with the observed value.

3.2 The radiation field

The radiation field used as input to CLOUDY is the spectral energy distribution generated by the evolutionary synthesis code developed by Leitherer and collaborators (Leitherer et al. 1999). The code includes the new set of stellar evolutionary models of the Geneva group (Schaller et al. 1992; Schaerer et al. 1993a,b; Charbonnel et al. 1993; Meynet et al. 1994), and the stellar atmospheres grid compiled by Lejeune et al. (1997), supplemented by the expanding spherical non-LTE models of Schmutz, Leitherer & Gruenwald (1992). The latter stellar atmosphere models are applied to stars with very strong stellar winds. The spectral energy distribution was generated using the Z=0.008 (Z \odot /2.5) metallicity tracks, assuming that stars and gas have the same metallicity. We assume two different star formation scenarios: instantaneous burst and continuous star formation at a constant rate. Different models are also computed with different assumptions about the IMF. The slope is Salpeter ($\alpha=2.35$), flatter ($\alpha=1.5$), or steeper ($\alpha=3.3$). The upper mass limit cut-off is set to 30, 60, 80 or 120 M \odot . The lower mass limit is fixed to 1 M \odot . However, photoionization models are not influenced by the lower limit mass cut-off if it is below 10 M \odot . The spectral energy distribution is normalized to an ionizing photon luminosity of log Q = 51.54 s⁻¹. This value is derived from the total H α flux measured in the image, after correcting by the mean extinction, $A_V = 0.5$ mag, derived by Churchwell & Goss (1999). We will check

below the compatibility of this normalization with the mass of the stellar cluster derived from the ultraviolet continuum luminosity.

3.3 The observational constraints

The emission lines were measured in our scanned spectrum of the nebula. The observed ratios have been corrected by the mean extinction, $c(H\beta)=0.22$, derived by Churchwell & Goss (1999). This value is in agreement with the reddening derived from the H γ /H β ratio measured in the scanned spectrum, when this ratio is corrected by the underlying stellar absorption. This extinction is lower than the values derived by Díaz et al. (1987), $c(H\beta)=0.3-0.4$; however, the extinction changes across NGC 604 (Maíz-Apellániz 1999). The de-reddened emission line ratios to be fitted by the photoionization models are included in Table 3. This table also includes the emission line ratios derived by Díaz et al. (1987) in several parts of the nebula, and those from an integrated spectrum in Maíz-Apellániz (1999). The range of values for each of these emission line ratios defines the tolerance that we accept for the difference between the observed and the predicted values from the models.

Following Stasińska & Schaerer (1999), we try to fit the strength of the emission lines, and also emission-line ratios indicative of the electron temperature ([O III]4363/5007), electron density ([S II]6717/6732) and ionization structure ([O III]5007/[O II]3727, [S III]9069/[S II]6716+6732). Another important observational constraint is the radius of the nebula. The H α image shows that the flux extends out to 200 pc of the center of the region; however, more than 90, 75 and 50 percent of the total flux is within the inner 140 pc, 100 pc and 60 pc radii, respectively (Fig. 3). Our determination of the core radius of the region is 80 pc.

3.4 Model results

We start by fixing the filling factor and the electron density by means of fitting the line ratios [S II]6717+6731/H β and [S II]6717/6731, and the radius of the nebula. [S II]6717+6731/H β is a good calibrator of the ionization parameter, because this ratio does not depend much on the IMF assumptions, on the star formation law or on the evolutionary state of the cluster (González Delgado et al. 1999a). Instead, this ratio depends on the filling factor, and for fixed geometry, ionizing photon luminosity and electron density, it depends on the ionization parameter ¶. The observed ratio, [S II]6717+6731/H $\beta \simeq 0.4$, indicates a filling factor $\phi \simeq 0.1$ (Fig. 6). Therefore, a large fraction of the volume of the region is filled with ionized gas; however, this gas is very tenuous because the *rms* electron density measured in the H α image is $\simeq 10$ cm⁻³, and the electron density in the S⁺ zone, derived from the definition of filling factor ($\phi = (N_e(rms)/N_e)^2$), is $N_e \simeq 30$ cm⁻³. The observed ratio [S II]6717/6731=1.4, indicates that the electron density is ≤ 100 cm⁻³. Models with a filling factor of 0.1 and $N_e = 30$

§ Notice, however, that the atomic parameters for the sulfur have changed in the intervening time

¶ Nonetheless, we should always be cautious when using sulfur dependent diagnostics, given the uncertainties about the atomic parameters and its not so well known ionization; also this calibration relies on the assumption of an ionization bounded nebula.

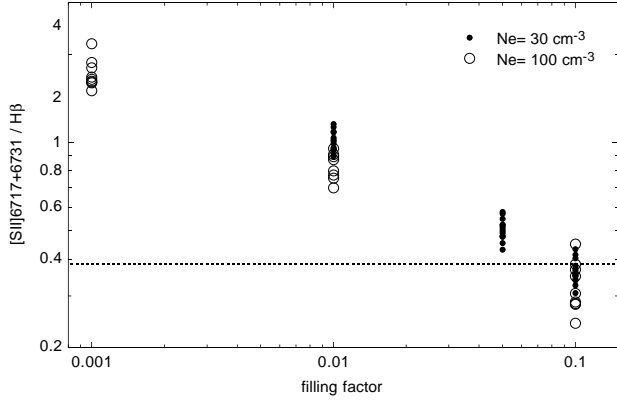


Figure 6. CLOUDY predictions of the emission-line ratio $[S II]6717+6731/H\beta$ as a function of the filling factor, taking as input the spectral energy distributions from the evolution of a cluster formed in an instantaneous burst. Ratios obtained with electron density of 100 cm^{-3} and 30 cm^{-3} are plotted as open and filled circles, respectively. The observed value is plotted as a horizontal line.

cm^{-3} predict well the observed $[S II]6717/6731$ ratio. If the electron density were as high as $N_e = 100 \text{ cm}^{-3}$, then the filling factor would have to be lower, $\phi = 0.01$, and in this case the values of $[S II]6717+6731/H\beta$ and $[S II]6717/6731$ predicted by the models are 0.9 and 1.3, respectively. These predictions are larger and smaller than the observed values, respectively. Furthermore, models with $\phi = 0.1$ and $N_e = 30 \text{ cm}^{-3}$ predict a Strömgren radius $\simeq 110 \text{ pc}$, in agreement with the radius derived from the $H\alpha$ surface brightness photometry. Models with $N_e = 100 \text{ cm}^{-3}$ predict a radius a factor two smaller than models with $N_e = 30 \text{ cm}^{-3}$. Therefore, we conclude that a filling factor $\phi \simeq 0.1$ and a density $N_e = 30 \text{ cm}^{-3}$ fit well the ratios $[S II]6717+6731/H\beta$ and $[S II]6717/6731$, and the size of the region.

The emission-line ratios $[O III]5007/H\beta$, $[O II]3727/H\beta$, $[O I]6300/H\beta$, and $[N II]6584/H\beta$ have been plotted as a function of the cluster age, using a filling factor $\phi = 0.1$ and an electron density $N_e = 30 \text{ cm}^{-3}$. To check whether the models also fit line ratios indicative of the structure of the region, we have plotted the η parameter, defined as $([O III]5007+4959/[O II]3727)/([S II]9069+9532)/[S II]6717+6731$, and the electron temperature predicted by the models as a function of the age. The parameter η is a measure of the softness of the radiation field (Vílchez & Pagel 1988). The models assume two different star formation laws, an instantaneous burst or continuous star formation at a constant rate, and different assumptions about the slope ($\alpha = 2.35, 1.50, 3.0$) and upper mass limit cut-off of the IMF ($M_{up} = 120, 80, 60, 30 M_\odot$).

Fig. 7 compares the observed emission line ratios with the prediction of continuous and instantaneous burst, for a Salpeter IMF and upper mass limit cut-off of $80 M_\odot$. The observed ratios are in better agreement with burst than with continuous star formation models (that predict high excitation lines and $[O I]6300/H\beta$ larger than observed). The continuous star formation scenario can be made compatible with the observed emission-line ratios if stars more massive than $50 M_\odot$ are not formed in the cluster; however, these

models predict significantly fewer numbers of Wolf-Rayet stars in the cluster. Thus, continuous star formation models cannot fit the emission-line ratios and predict the existence of Wolf-Rayet stars simultaneously.

Fig. 8 compares the observed emission line ratios with the prediction of an instantaneous burst, for different assumptions of the IMF upper mass limit cut-off. Models with $M_{up} = 30 M_\odot$ predict high excitation lines (low excitation lines) ratios which are much lower (higher) than the observed values. Thus, similar results are obtained if $M_{up} \leq 50 M_\odot$. Burst models with $M_{up} \geq 60 M_\odot$ fit the emission-line ratios if the age of the cluster is 2.5–3 Myr or 4.5–4.8 Myr. However, if $M_{up} = 60 M_\odot$, Wolf-Rayet stars only appear in the cluster if it is 4–5 Myr old. Models with $M_{up} = 120 M_\odot$ and $80 M_\odot$ give similar results after the first 2 Myr, and the same behaviour with age. The electron temperature, η and the emission-line ratios, all indicate that massive stars ($M_{up} \geq 80 M_\odot$) have to be present in the cluster, and that the cluster is $\simeq 3 \text{ Myr}$ or $\simeq 4.5 \text{ Myr}$ old. Further constraints on the upper mass limit cut-off will be imposed by the relative number of Wolf-Rayet with respect to O stars in the cluster.

Burst models have been computed also for different values of the IMF slope ($\alpha = 2.35, 3.0$ and 1.5). The behaviour of the emission line ratios with the age is very similar for these three values of the IMF slope (Fig. 9). The observed ratios indicate an age $\simeq 3 \text{ Myr}$ or 4.5 Myr , and cannot discriminate between the different values of the slope. Further constraints on the IMF slope will come from the WR/O ratio. This point will be discussed further in section 6.

4 MODELING THE H BALMER AND HE I ABSORPTION LINES

The optical continuum of an RH II is dominated by early-type stars. The spectra of O and B stars are characterized by strong H Balmer and He I absorption lines, with very weak metallic lines formed in the photosphere of these stars (Walborn & Fitzpatrick 1990). The H Balmer and He I recombination nebular emission lines are superposed on the corresponding photospheric lines. However, the higher order terms of the Balmer series and some of the He I lines can be detected in absorption and the lower terms of the Balmer series can show absorption wings. The detection of these absorption features depends on the spectral and spatial resolution of the observations, on the spatial distribution of the stellar cluster with respect to the nebular emission, and on the evolutionary state of the stellar cluster. These photospheric features have been detected in a spectrum of NGC 604 (Fig. 5) because it corresponds to the zone of the nebular hole where the core of the central cluster is located, so it maximizes the contrast of the stellar with respect to the nebular contributions (see Fig. 2). In this section we will constrain the evolutionary state of NGC 604 and the IMF using the profile of the higher-order terms of the H Balmer series and the strength of some of the He I lines in absorption.

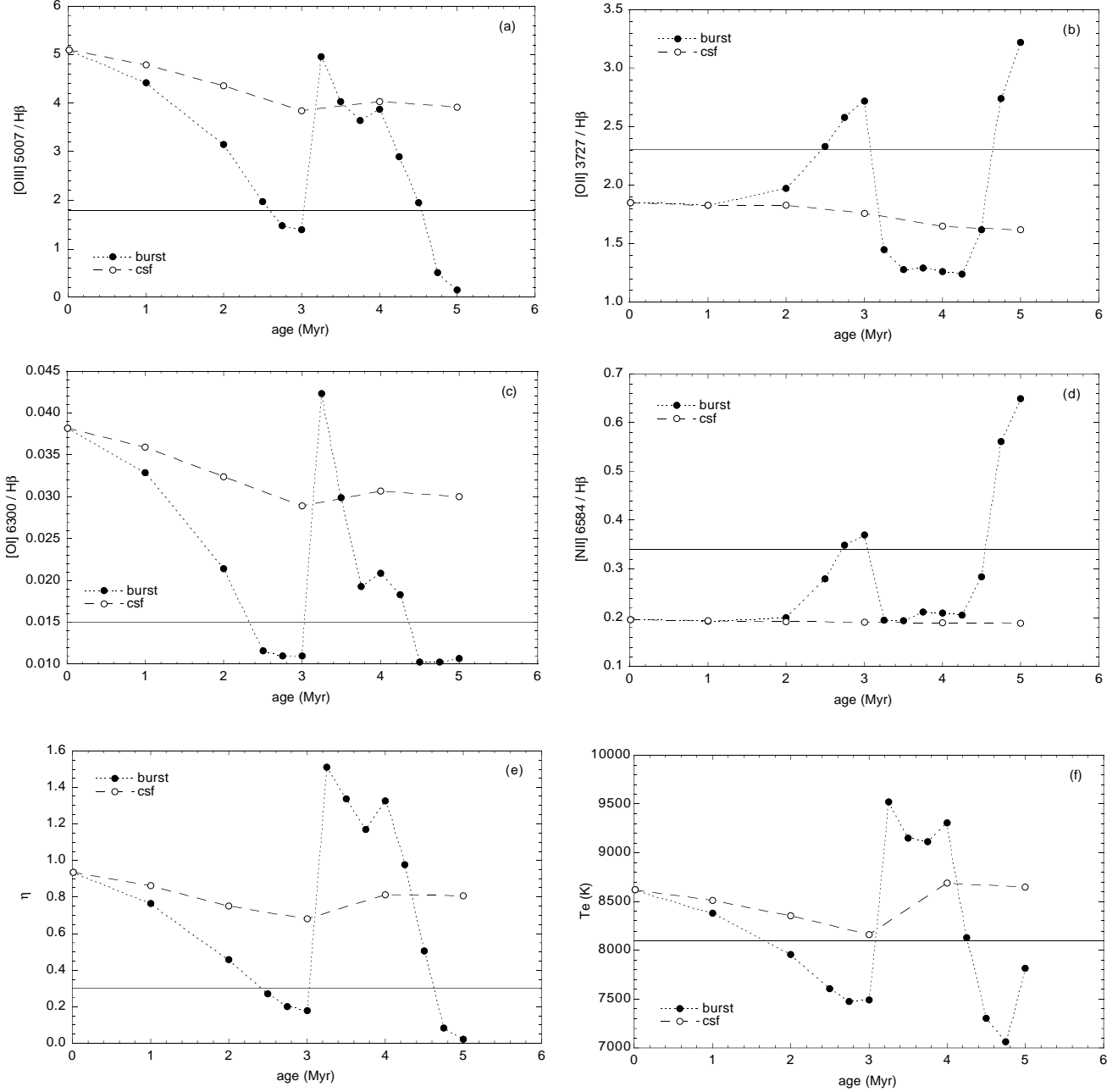


Figure 7. Predicted emission-line ratios, η parameter and the electron temperature as a function of the cluster age, for an instantaneous burst (filled symbols) and continuous star formation (open symbols). The models assume that the mass of the cluster is distributed following a Salpeter IMF between 1 and 120 M_{\odot} . The filling factor is 0.1 and the electron density 30 cm^{-3} . The observed values are represented by an horizontal line.

4.1 Description of the models

González Delgado et al. (1999b) have computed evolutionary stellar population synthesis models that predict the photospheric absorption H Balmer and HeI lines, between 3700 and 5000 Å, for a single-metallicity stellar population. The models, which are optimized for galaxies with active star formation, synthesize the profiles of the H Balmer series ($H\beta$, $H\gamma$, $H\delta$, $H8$, $H9$, $H10$, $H11$, $H12$ and $H13$) and the

HeI absorption lines (HeI $\lambda 4922$, HeI $\lambda 4471$, HeI $\lambda 4388$, HeI $\lambda 4144$, HeI $\lambda 4121$, HeI $\lambda 4026$, HeI $\lambda 4009$ and HeI $\lambda 3819$), with a spectral sampling of 0.3 Å pixel^{-1} , for a burst and for continuous star formation at a constant rate. They use a stellar library that includes NLTE absorption profiles for stars hotter than 25000 K, and LTE profiles for lower temperatures. The temperature and gravity coverage is $4000 \leq T_{\text{eff}} \leq 50000 \text{ K}$, and $0.0 \leq \log g \leq 5.0$, respectively (González Delgado & Leitherer 1999). The models assume

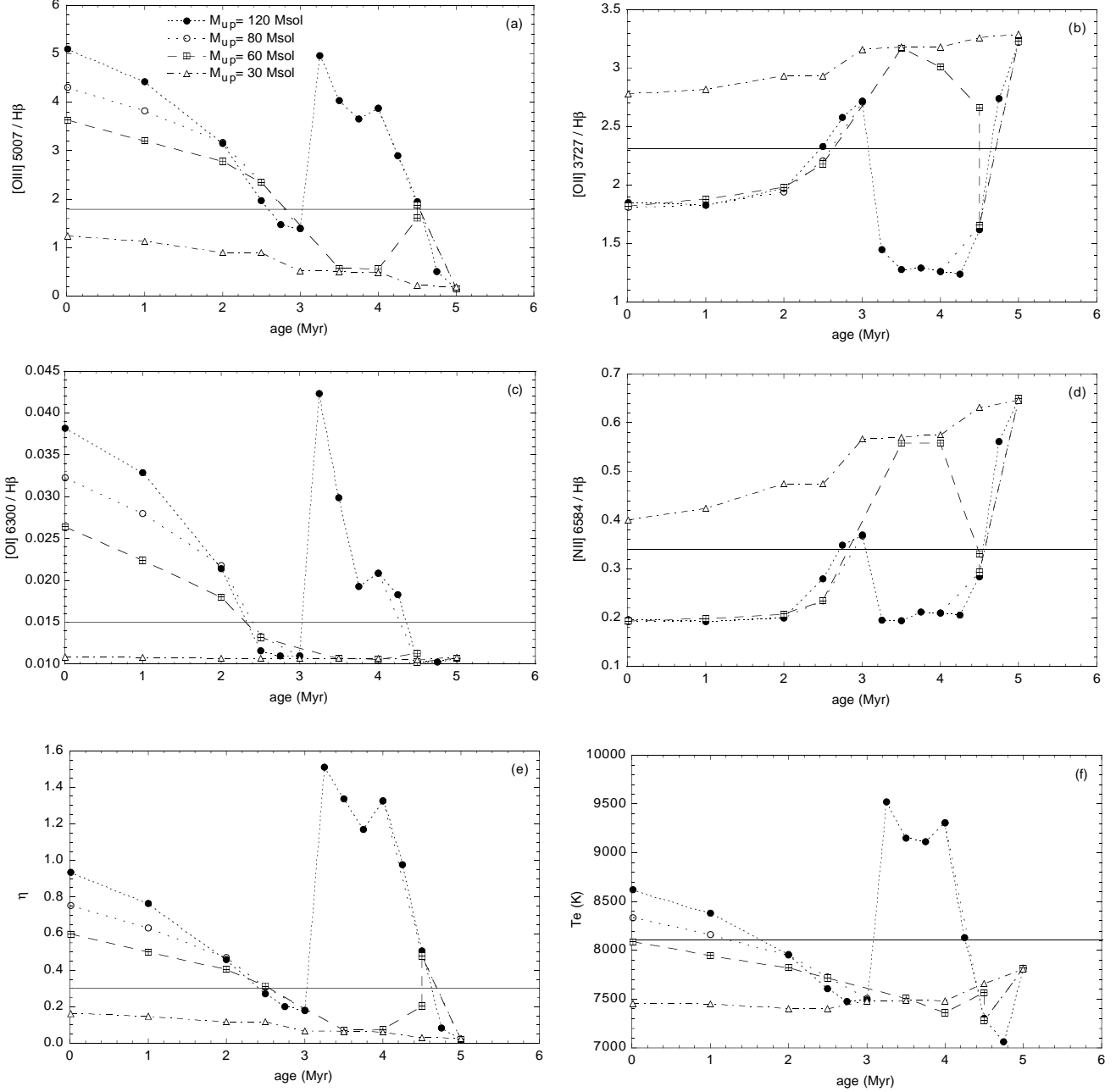


Figure 8. As Figure 7, but for an instantaneous burst with a Salpeter IMF upper mass limit cut-off 120 M_{\odot} (filled circles), 80 M_{\odot} (open circles), 60 M_{\odot} (squares), and 30 M_{\odot} (open triangles).

that stars evolve from the main sequence following the evolutionary tracks of the Geneva group (Schaller et al. 1992; Schaerer et al. 1993a,b; Charbonnel et al. 1993; Meynet et al. 1994). The strength of the Balmer and HeI lines is sensitive to the age after the first 3 Myr of evolution, and sensitive to the IMF if the age is younger than 3–4 Myr. Models assume that stars have a metallicity $Z = 0.008$, and make different assumptions about the IMF slope ($\alpha = 1.5, 2.35$ and 3.0), and upper mass limit cut-off ($M_{up} = 80 M_{\odot}$ and $30 M_{\odot}$). For the purpose of this paper, the range of ages computed spans from 0 to 10 Myr.

4.2 Model Results

We use the equivalent width of HeI $\lambda 4388$, $\lambda 4026$, and $\lambda 3819$, and the wing absorption profiles of H β , H γ , H δ , H8, H9 and H10 to constrain the age, IMF and star formation law. HeI $\lambda 4388$, $\lambda 4026$, and $\lambda 3819$ are detected in absorption, because the corresponding nebular emission lines have equivalent widths that are at least a factor 3 weaker than the nebular emission in HeI $\lambda 4471$ (González Delgado et al. 1999b). Note that HeI $\lambda 4471$ is only partially filled with the nebular emission; therefore, the nebular emission of the

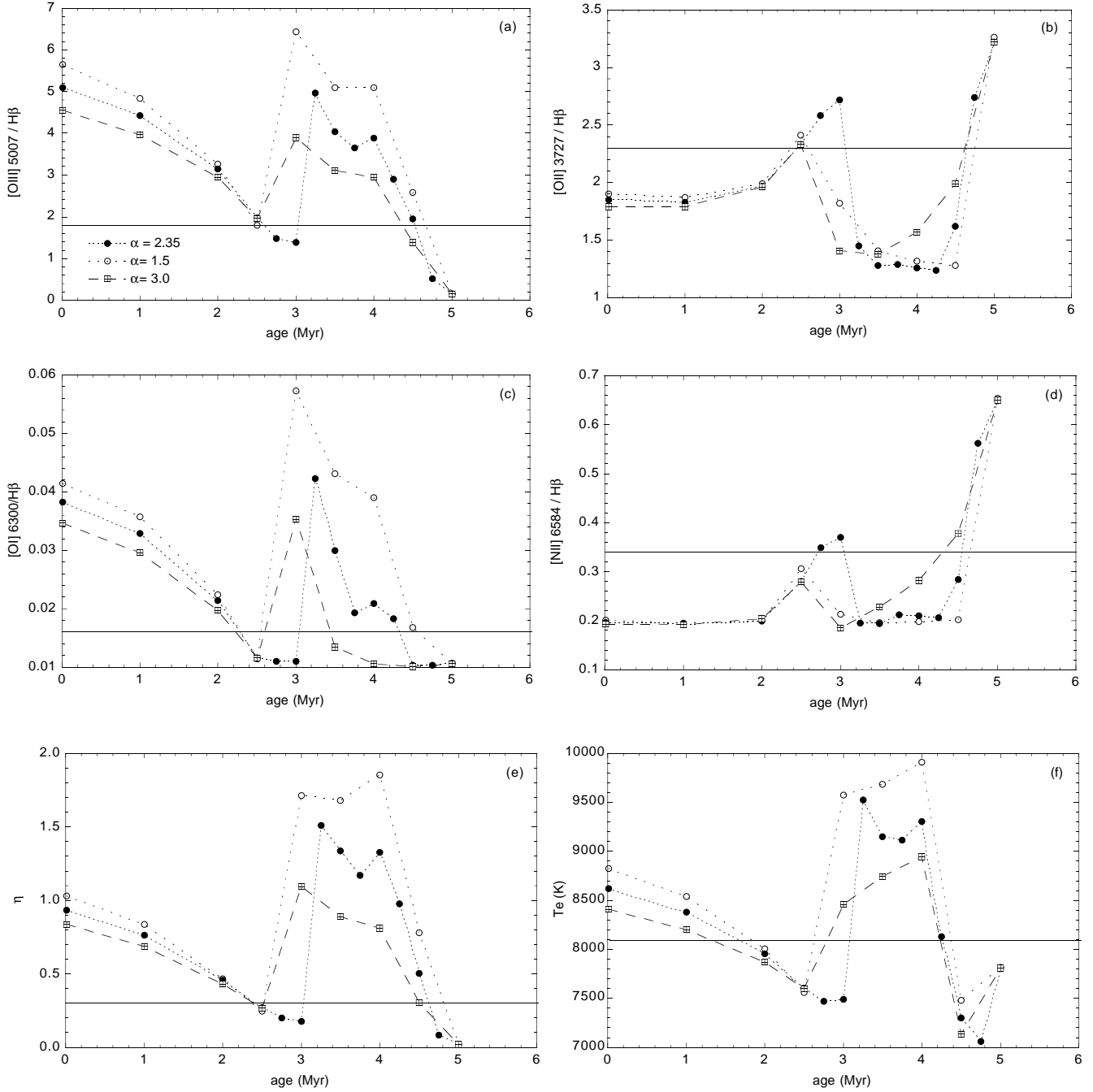


Figure 9. As Figure 7, but for an instantaneous burst with an IMF slope $\alpha=2.35$ (Salpeter, filled circles), $\alpha=1.5$ (open circles) and $\alpha=3.0$ (squares) and upper mass limit cut-off $80 M_{\odot}$.

lines He I $\lambda 4388$, He I $\lambda 4026$ and He I $\lambda 3819$ is $\simeq 0$, and the equivalent widths of these absorption features represent well the strength of the stellar continuum radiation of the cluster. The equivalent widths of these lines, He I $\lambda 4388$, He I $\lambda 4026$ and He I $\lambda 3819$, measured in the spectrum of Fig. 5 are 0.32, 0.55 and 0.26 Å, respectively. Their strength is compatible with continuous star formation and with burst models 3 Myr old (Fig. 10). However, He I lines can constrain the IMF. Models with an IMF steeper than Salpeter or with $M_{\text{up}} = 30 M_{\odot}$ predict He I lines stronger than ob-

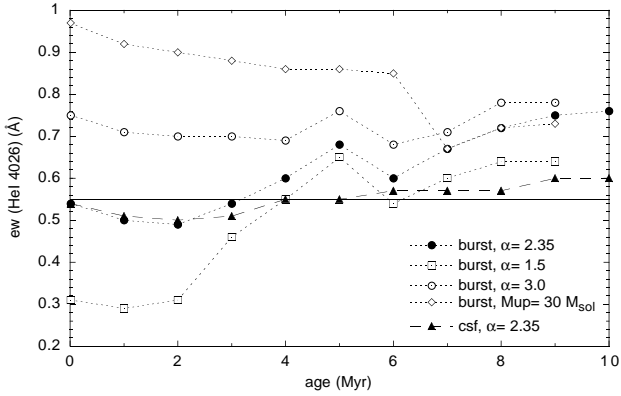
served. The strengths of the lines are compatible with a 3 to 4 Myr old burst formed following a Salpeter or slightly flatter IMF ($\alpha = 1.5$, Fig. 10). The absorption wings of the Balmer lines are also compatible with burst models 3 Myr old, with Salpeter or slightly flatter IMF ($\alpha = 1.5$, Fig. 11).

Table 3. Emission line ratios, normalized to $H\beta=1$.

Line	Observations					Models		
	(1)	A	C	D	B	2.5 Myr	3.0 Myr	3.5 Myr
[O II] 3727	2.3	2.08	2.49	1.61	2.00	2.3	2.7	1.3
[Ne III] 3869	0.11	0.15	0.26	0.13	0.07	0.08	0.034	0.29
[O III] 4363	0.0054	0.0062	≤ 0.004	0.087	0.0063	0.0052	0.0033	0.024
[O III] 5007	1.8	2.69	0.97	2.55	1.8	2.0	1.4	4.0
[O I] 6300	—	0.015	—	0.01	0.02	0.012	0.011	0.03
[N II] 6584	0.34	0.30	0.51	0.27	0.31	0.28	0.37	0.19
[S II] 6716	0.23	0.14	0.31	0.16	0.16	0.19	0.21	0.22
[S II] 6732	0.16	0.11	0.23	0.11	0.13	0.14	0.15	0.16
[S III] 9069	0.40	0.33	0.25	0.51	0.40	0.40	0.40	0.34
[O III] 4363/5007	0.0030	0.0023	≤ 0.0041	0.034	0.0035	0.0026	0.0024	0.006
[S II] 6717/6732	1.4	—	—	—	—	1.4	1.4	1.4
η'	0.3	—	—	—	—	0.27	0.18	1.3

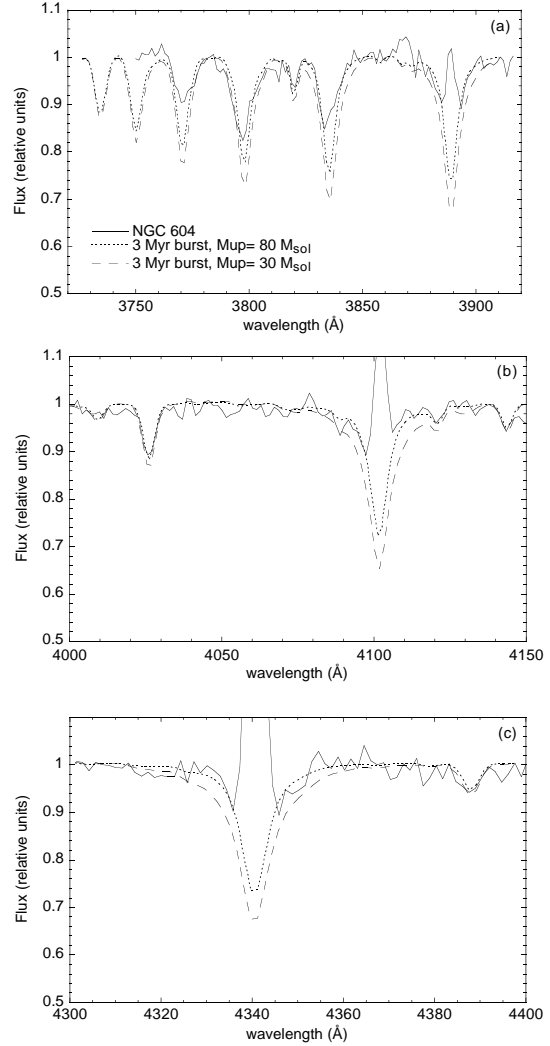
(1): line ratio measured in our scanned spectrum or the integrated spectrum of Maíz-Apellániz (1999).

A, B, C and D are the line ratios in different parts of the nebula, from Díaz et al. (1987)

**Figure 10.** Predicted equivalent widths of the He I $\lambda 4026$ stellar absorption line as a function of the age for continuous star formation (filled triangles) and burst (filled circles) models, assuming a Salpeter IMF between 1 and $80 M_{\odot}$. Burst models are computed for different IMF slopes, $\alpha=1.5$ (squares), 3.0 (open circles), and upper mass limit cut-offs, $M_{up}=30 M_{\odot}$ (open diamonds). The observed value is plotted as an horizontal line. The equivalent widths of He I $\lambda 4388$, $\lambda 3819$ are smaller than that of $\lambda 4026$ and do not add further constraints, so they are not shown for the sake of clarity.

5 MODELLING THE ULTRAVIOLET STELLAR LINES

The ultraviolet light from an RH II is dominated by O stars. These hot stars develop strong wind stellar lines due to the radiation pressure in ultraviolet resonance lines (Morton 1967). As a result, all the strong ultraviolet lines (e.g. O VI $\lambda 1034$, N V $\lambda 1240$, Si IV $\lambda 1400$, C IV $\lambda 1550$ and N IV $\lambda 1720$) show a blueshifted absorption (about $2000\text{--}3000 \text{ km s}^{-1}$) or a PCygni profile. The shape of the profile reflects the stellar mass-loss rate, which is related to the stellar luminosity, and thus to the stellar mass. Most of the ultraviolet spectra of RH II are dominated by absorption features (Rosa et al. 1984; Vacca et al. 1995; Mas-Hesse & Kunth 1999), without any nebular emission, which is very similar to those of star-

**Figure 11.** The normalized spectrum of Fig. 5 (full line). Also plotted are the synthetic normalized spectra of a 3 Myr old instantaneous burst with a Salpeter IMF, and with $M_{up} = 80 M_{\odot}$ (dotted line) and $30 M_{\odot}$ (dashed line). Models are degraded to the spectral resolution of the observations.

burst galaxies^{||}. Most of these lines are formed in the stellar winds of the massive stars that belong to the starburst. The profile of these lines reflects the stellar massive content in the starburst; therefore, they depend on the IMF and star formation law (Leitherer, Robert & Heckman 1995). In this section, we constrain the evolutionary state and the IMF of NGC 604 by means of fitting the profiles of the ultraviolet stellar lines Si IV and C IV.

5.1 Description of the models

Evolutionary stellar population models have been computed with the code Starburst 99 (Leitherer et al. 1999). The code uses a stellar library of *IUE* ultraviolet spectra of O, B and Wolf-Rayet stars (Robert, Leitherer & Heckman 1993). The spectral resolution of the O and Wolf-Rayet stars observed is 0.75 Å. These stars are located in the solar neighborhood. However, the evolutionary models computed here assume that the stars evolve from the main sequence following the evolutionary track at $Z = 0.008$. Models are computed for instantaneous bursts between 0 and 10 Myr, and for continuous star formation lasting 10 Myr, and different assumptions about the slope ($\alpha=2.35, 3.0$ and 1.5) and upper mass limit cut-off ($M_{\text{up}} = 120, 80, 60$ and $40 M_{\odot}$) of the IMF. The model spectra are smoothed to the *IUE* spectral resolution of the observations of NGC 604, which is 6 Å.

5.2 Model results

The strongest wind stellar features in the spectra of NGC 604 are N V $\lambda 1240$, Si IV $\lambda 1400$, C IV $\lambda 1550$, He II $\lambda 1640$, and N IV $\lambda 1720$. These features are present in all the spectra of NGC 604; however, for this analysis we use the average spectrum of those at PA=149°, 136° and 159°, and the spectrum at PA=32°, because they have the best signal to noise ratio. The evolutionary state, the star formation law and the IMF in NGC 604 is constrained with the profiles of these lines.

He II shows a broad emission profile in Wolf-Rayet and O3–O5 supergiant stars; N IV shows a PCygni profile in Wolf-Rayet stars; N V and C IV show strong PCygni profiles in all O stars, and Si IV only in O supergiants. Thus, the profile of these lines in the integrated spectrum of a starburst depends strongly on the stellar content and age of the stellar cluster. In particular, Si IV shows a strong PCygni profile if the cluster formed in an instantaneous burst and its age is between 3 and 5 Myr, because within this age interval the ultraviolet light is dominated by O blue supergiants. On the other hand, the profile of C IV depends strongly on the IMF. It shows a strong PCygni profile if stars more massive than $60 M_{\odot}$ are formed in the cluster, and if the slope of the IMF is flatter than $\alpha=3.0$.

The spectrum of NGC 604 indicates that its stellar population must be dominated by massive, young O stars; thus, the stellar cluster must be young and of short duration. Continuous star formation models can be ruled out because they show Si IV weaker than observed (Fig. 12). In these models the line is diluted because the fraction of O supergiants with

respect to the total number of O stars is lower in the continuous star formation than in the instantaneous burst models. The strength of Si IV in NGC 604 indicates that it is an instantaneous burst. The age of the burst has to be between 3 to 5 Myr, because bursts younger than 3 Myr or older than 5 Myr have very few O supergiants, and thus very weak Si IV (Fig. 13). On the other hand, from the strength of C IV we can exclude instantaneous bursts with $M_{\text{up}} \leq 60 M_{\odot}$ (Fig. 14), and IMF steeper than $\alpha=3.0$ (Fig. 15). Therefore, we conclude that continuous star formation and instantaneous burst models with few very massive stars can be ruled out. The wind lines are compatible with an instantaneous burst, formed following a Salpeter or slightly flatter IMF, with upper mass limit cut-off higher than $60 M_{\odot}$. A 3 Myr instantaneous burst with Salpeter and $M_{\text{up}} \geq 80 M_{\odot}$ fits well the profile of the wind stellar lines.

6 THE MASSIVE STELLAR CONTENT OF NGC 604

We derive the massive stellar population in NGC 604 from the ultraviolet continuum luminosity, comparing the observations with the predictions of synthetic models. The number of Wolf-Rayet stars are derived from the luminosity of the He II $\lambda 1640$ line. The stellar content derived in this way is compared with that derived from *HST* photometry of stars in NGC 604. However, we need first to estimate the extinction.

6.1 Extinction estimates

Leitherer & Heckman (1995) have shown that the ultraviolet continuum arising from a young starburst (age ≤ 10 Myr) has a spectral index, β ($F_{\lambda} \propto \lambda^{\beta}$), which is independent of the IMF, star formation law and metallicity. Thus, any deviation from the predicted value, $\simeq 2.5$ for a 3 Myr instantaneous burst, could be attributed to reddening.

The ultraviolet continuum flux distribution of the *IUE* spectra of NGC 604 shows evidence of reddening, because after correcting by Galactic extinction, $E(B - V) = 0.03$ (McClure & Racine 1969), the spectra are flatter than the spectral energy distribution predicted by the evolutionary synthesis models. Massey & Hutchings (1983), analysing *IUE* spectra of H II regions in M33, conclude that the M33 extinction curve is significantly different from that of the Galaxy, because the spectra of the H II regions show very weak 2200 Å interstellar absorption dip, resembling those of the LMC and SMC. Therefore, we use the LMC curve to match the observed spectra with the spectral energy distribution of a 3 Myr old instantaneous burst. The $E(B - V)$ derived is 0.1 for the spectrum at PA=32°, and 0.12 for the average spectrum of those at PA=136°, 159° and 149°. These values are in agreement with those derived by Massey & Hutchings (1983). However, the extinction can be 0.03 higher than the values above if it is derived comparing the observed spectra with the spectral energy distribution predicted including only the stellar contribution. This is due to the nebular contribution being dominated by the two-photon continuum emission that peaks at ~ 1500 Å. If the nebular continuum is not included, the spectral energy distribution is steeper and a higher extinction is required to match the observed

^{||} One important exception is knot A in the RH II NGC 2363 (Drissen et al. 2000), so young that the effect of winds is not yet reflected in its uv spectrum.

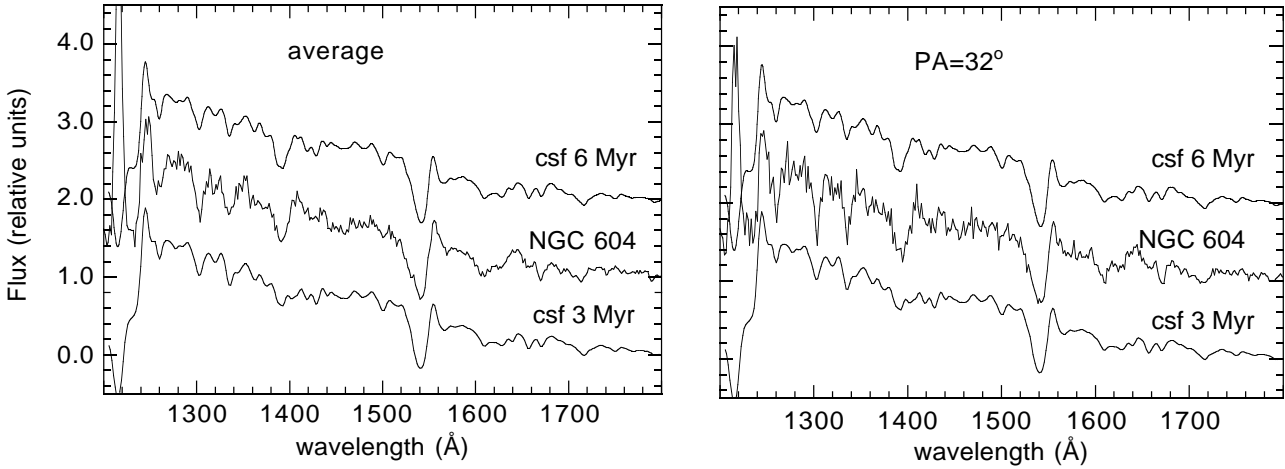


Figure 12. *IUE* spectra of NGC 604 (normalized at 1800 Å), dereddened by a galactic extinction $E(B - V) = 0.03$ using the MW extinction law, and by an intrinsic extinction $E(B - V) = 0.12$ using the LMC extinction law, for the average spectrum (a), and and intrinsic $E(B - V) = 0.1$ for the spectrum at $PA=32^\circ$ (b). Synthetic continuous star formation models for 3 and 6 Myr are plotted in relative units. The IMF is Salpeter with $M_{\text{up}} = 80 M_\odot$. Models are smoothed to the resolution of the observations, 6 Å.

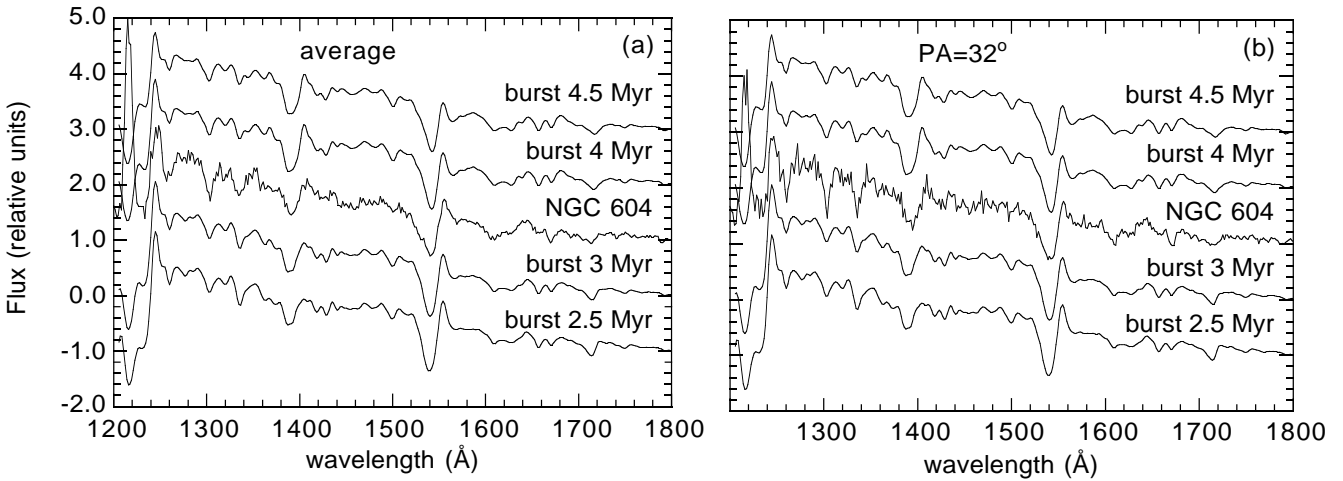


Figure 13. As in Fig. 12 for an instantaneous burst 2.5, 3, 4 and 4.5 Myr old.

and predicted ultraviolet flux distribution. The reason to do this new estimation is because the nebula is more extended than the *IUE* aperture; thus, only a fraction of the nebular continuum contributes to the *IUE* aperture.

We have estimated also the extinction using the Calzetti, Kinney & Storchi-Bergmann (1994) extinction law. This is an empirical extinction curve derived for starbursts, which is very similar to the MW extinction law but it does not show the 2200 Å bump. Using this curve, we estimate $E(B - V) = 0.2$ to match the observed spectra and the spectral energy distribution predicted by the models.

To distinguish between these two results, we compare the spectral energy distribution predicted by the evolutionary models with that of NGC 604. We build the spectral energy distribution of NGC 604 from the ultraviolet to near-

infrared using the SWP+LWR *IUE* spectrum at $PA=110^\circ$ plus that at $PA=149^\circ$, and the average optical spectra scanning the inner 11×60 arcsec (at $PA=120^\circ$), and 14×60 arcsec (at $PA=60^\circ$). We use the *B* (F439W) and *I* (F814W) *HST*+WFPC2 images to flux calibrate the optical spectra, because the mode in which the scanning was performed precludes an accurate absolute flux calibration based only on the ground-based observations. The resulting optical and ultraviolet spectra are normalized dividing by the flux at 2900 Å. Then, the spectra are dereddened by $E(B - V) = 0.1$ using the LMC extinction law, and by $E(B - V) = 0.2$ using the Calzetti et al. (1994) extinction law. Even though apparently the spectra dereddened with Calzetti's law seem to match better the spectral energy distribution, a change in the scaling calibration factor of only 10 percent (larger than

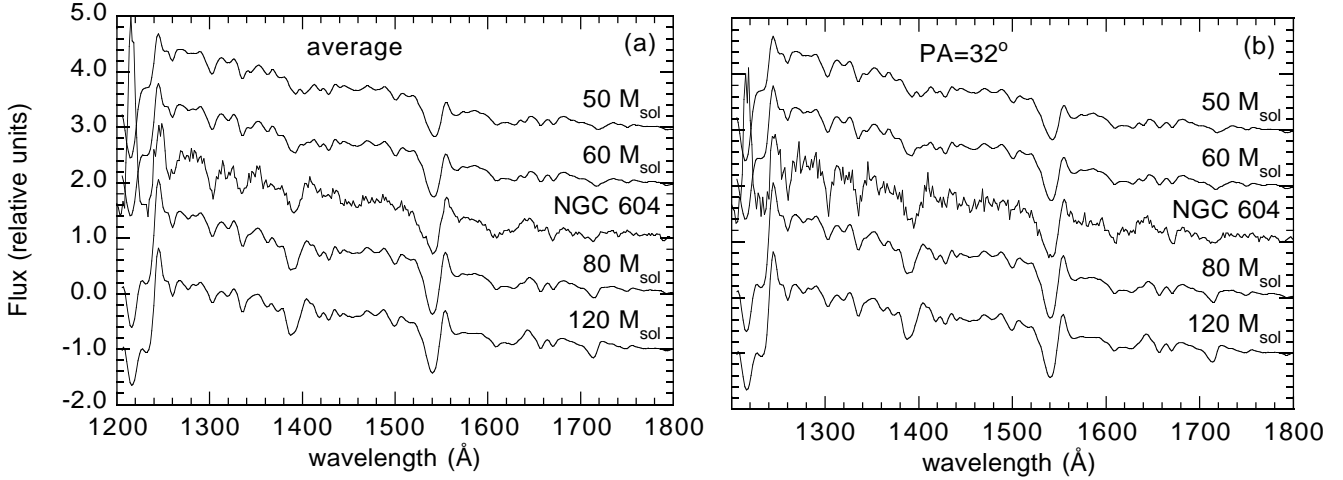


Figure 14. As Fig. 12 for an instantaneous burst 3 Myr old. The IMF is Salpeter and the upper mass limit cut-off as labelled.

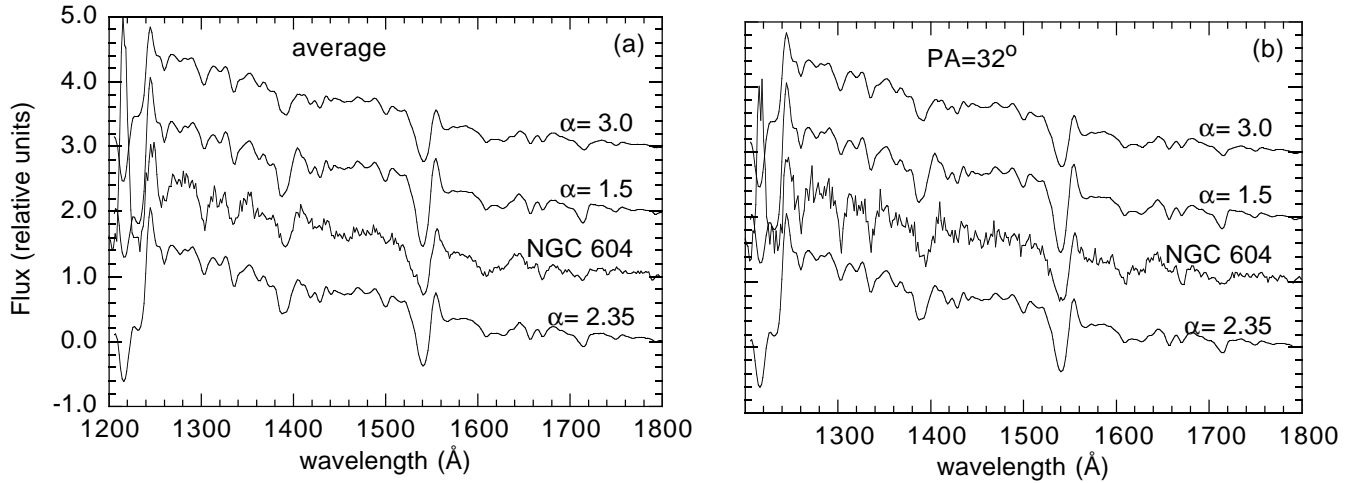


Figure 15. As Fig. 14. The IMF slope is $\alpha = 2.35, 1.5$ and 3.0 , and $M_{\text{up}} = 80 M_{\odot}$.

that used) gives a better match with the spectrum dereddened by the LMC law. Thus, given the uncertainties in the flux calibration of the ground-based optical spectra, we cannot really distinguish between these two extinction laws.

6.2 The number of O stars and W/O ratio

We assume that the total ultraviolet flux of the region is approximately the sum of the fluxes at $\text{PA}=110^{\circ}$ and at $\text{PA}=149^{\circ}$. After correcting by Galactic extinction, the flux at 1500 \AA is $5.1 \times 10^{-13} \text{ erg s}^{-1} \text{ cm}^{-2} \text{ \AA}^{-1}$. The intrinsic luminosity^{★★} is $10^{38.16} \text{ erg s}^{-1} \text{ \AA}^{-1}$ ($10^{38.32} \text{ erg s}^{-1} \text{ \AA}^{-1}$)

★★ Note that this luminosity and the quantities derived in Table 4 should be almost a factor two lower if the total ultraviolet flux is equal to the flux of only one of the *IUE* apertures, or to that

if the flux is corrected by $E(B - V) = 0.12$ (0.2) using the LMC (Calzetti et al. 1994) extinction law.

The mass of the cluster, the ionizing photon luminosity and the number of O stars predicted by the evolutionary synthesis models are given in Table 4. These quantities indicate that very massive stars must be present in the cluster and that it is very young. In fact, instantaneous bursts older than 3.5 Myr predict an ionizing photon luminosity which is at least a factor 3 lower than the value derived from the $\text{H}\alpha$ flux, which is $\log Q = 51.54 \text{ (s}^{-1}\text{)}$. In contrast, a $\simeq 3$ Myr instantaneous burst (with $M_{\text{up}} \geq 80 M_{\odot}$) reproduces well the ionizing photon luminosity^{††}. These models predict

measured in the F170W HST image, $L_{1700} \simeq 7 \times 10^{37} \text{ erg s}^{-1} \text{ \AA}^{-1}$.

†† However the values of Q predicted are still a factor 1.5 lower than the photon luminosity derived from the $\text{H}\alpha$ flux, suggesting

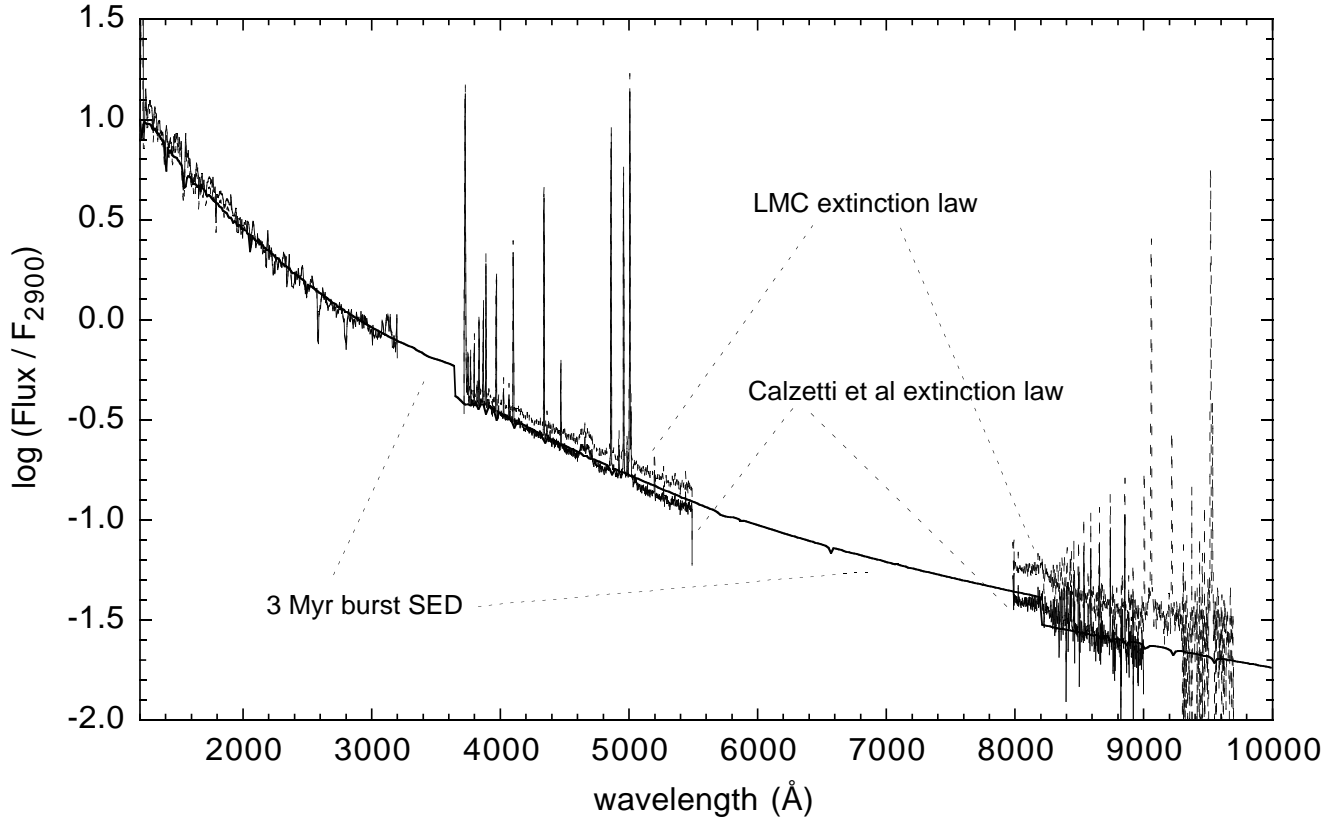


Figure 16. Spectral energy distribution of an instantaneous burst 3 Myr old, normalized at 2900 Å, compared with ultraviolet plus optical spectra dereddened by $E(B - V) = 0.1$ using the LMC extinction law, and by $E(B - V) = 0.2$ using the Calzetti et al. (1994) extinction law.

a mass of the stellar cluster that ranges between 0.1 and $2 \times 10^5 M_{\odot}$, depending on the assumption about the upper mass limit cut-off and slope of the IMF. The number of O stars ranges between 150 and 215 (if $M_{\text{up}} \geq 80 M_{\odot}$), which is in agreement with the number of O stars (186) reported by Hunter et al. (1996).

The slope and upper mass limit cut-off of the IMF can also be constrained with the observed Wolf-Rayet over O ratio, WR/O. *HST* images of the NGC 604 cluster have detected 14 Wolf-Rayet or Of candidates (Drissen et al. 1993). Thus, $\text{WR/O} \sim 0.075$. This ratio is very high, suggesting that the cluster is young (3–3.5 Myr), and that it must contain very massive stars. Instantaneous burst models with the IMF slope steeper than Salpeter or $M_{\text{up}} \leq 80 M_{\odot}$ predict a ratio much lower than 0.075 (Fig. 17). Models with IMF flatter than Salpeter or with upper mass limit cut-off as high as $120 M_{\odot}$ reproduce well the observed value.

that other sources in addition to the central cluster contribute to the ionization of the gas, and/or that the extinction is higher than $E(B - V) = 0.1$. Note that if $\log L_{1500} = 38.32 \text{ erg s}^{-1} \text{ Å}^{-1}$, then all the quantities derived in Table 4 should be a factor $\simeq 1.5$ larger.)

6.3 Deposition of kinetic energy in the interstellar medium

Massive stars not only interact with the interstellar medium via their radiation, but also depositing kinetic energy via their stellar winds. The energy released during their lifetime is comparable to that deposited by a supernova event (Leitherer, Robert & Drissen 1992). The evolutionary state and the stellar content derived above for NGC 604 suggests that the massive stars in NGC 604 can release enough kinetic energy to form many of the filaments and expanding shell structures observed in the region.

Yang et al. (1996) have reported the properties of five shells; these have expansion velocities that range between 40 and 125 km s^{-1} , and sizes between 35 and 125 pc (see also Sabalisk et al. 1995). The wind power required to form these bubbles ranges between $2 \times 10^{37} \text{ erg s}^{-1}$ and $9 \times 10^{38} \text{ erg s}^{-1}$, with a sum total of $\simeq 10^{39.25} \text{ erg s}^{-1}$.

We estimate the wind power produced by the stellar cluster in NGC 604 using Starburst99 (Table 4). For an instantaneous burst, the wind power ranges between $3 \times 10^{37} \text{ erg s}^{-1}$ and $4 \times 10^{38} \text{ erg s}^{-1}$, depending on the assumptions about the slope and massive cut-off of the IMF. Thus, the energy released by winds in NGC 604 is not enough to explain the formation of the five shells; however, it can explain the formation of the central hole (shell number 3) and shell

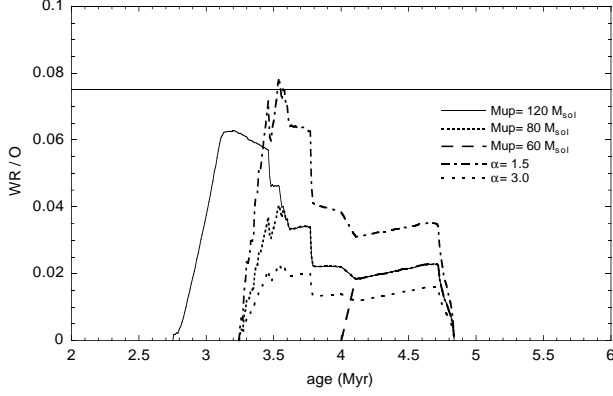


Figure 17. Ratio of the number of Wolf-Rayet with respect to the total O stars as a function of age, for different assumptions of the IMF slope, $\alpha = 3.0, 2.35$ and 1.5 ($M_{\text{up}} = 80 M_{\odot}$), and upper mass limit cut-off, $M_{\text{up}} = 120, 80$ and $60 M_{\odot}$ ($\alpha = 2.35$).

Table 4. Model predictions for massive stars and energy released.

age (Myr)	α	M_{up} (M_{\odot})	$\log Q$ (ph s^{-1})	Mass ($10^5 M_{\odot}$)	No.O	$\log P_w$ (erg s^{-1})
$\log L_{1500} = 38.16 \text{ erg s}^{-1} \text{ \AA}^{-1}$						
3.0	2.35	80	51.28	0.47	209	37.98
3.5	2.35	80	51.20	0.43	189	38.59
4.0	2.35	80	51.10	0.51	218	38.38
4.5	2.35	80	51.02	0.62	244	38.50
5.0	2.35	80	50.86	0.72	262	37.36
3.0	2.35	120	51.40	0.36	164	38.60
3.5	2.35	120	51.21	0.44	186	38.99
4.0	2.35	120	51.10	0.54	220	38.39
4.5	2.35	120	51.02	0.65	247	38.51
5.0	2.35	120	50.86	0.74	258	37.36
3.0	1.50	80	51.28	0.13	180	38.05
3.5	1.50	80	51.23	0.12	152	38.76
4.0	1.50	80	51.11	0.17	199	38.55
4.5	1.50	80	51.06	0.24	239	38.67
5.0	1.50	80	50.85	0.31	267	37.41
3.0	3.00	80	51.24	2.00	215	37.45
3.5	3.00	80	51.14	1.90	198	37.96
4.0	3.00	80	51.05	2.00	210	37.78
4.5	3.00	80	50.97	2.20	228	37.92
5.0	3.00	80	50.74	1.90	187	36.84

number 4 (see fig. 2 in Yang et al. 1996), that encircles the core of NGC 604 cluster (cf. Fig. 2). The wind power required by these two bubbles is $5 \times 10^{37} \text{ erg s}^{-1}$ and $2 \times 10^{37} \text{ erg s}^{-1}$, respectively.

SUMMARY AND CONCLUSIONS

The main goal of this work is to constrain the evolutionary state of the giant HII region NGC 604. For this purpose, we have analyzed the integrated ultraviolet spectra taken by *IUE*, and optical ground-based spectra of the region. The data are interpreted using evolutionary synthesis models optimized for star forming regions. These data are

complemented with ultraviolet and H α images taken by *HST* with the WFPC2.

The ultraviolet image shows that the ionizing cluster is spatially spread in the inner 20×20 arcsec, with the core of the cluster within a central nebular hole shell structure. The optical spectrum, as it is well known, is dominated by nebular emission lines from the surrounding photoionized medium. In contrast, the ultraviolet spectrum of the region is dominated by absorption lines formed in the stellar winds of massive stars. However, other photospheric stellar lines (the high order terms of the Balmer series and He I lines) are detected at optical wavelengths near the Balmer jump. The spatial distribution of the stellar cluster with respect to the nebular emission, allows to detect these lines in absorption in a spectrum corresponding to the inner 4 arcsec of the region, where the stellar light is maximized with respect to the nebular contribution.

The evolutionary state and the massive stellar content of the region is derived in a self-consistent way using evolutionary synthesis and photoionization models, applied to the ultraviolet resonance wind stellar lines, to the nebular emission-lines and to the higher-order terms of the Balmer series and He I lines in absorption. The three techniques applied suggest that the central ionizing cluster of NGC 604 is very young, 3 Myr old, with no evidence for an age spread. The overall properties suggest that the massive stars in the cluster were formed following a Salpeter or flatter IMF, with presence of stars more massive than $80 M_{\odot}$.

Particular results from the modelling of the nebular emission lines include:

- The nebula is well described by a sphere of inner radius 20 pc and outer radius 110 pc (determined by the ionization front). This value is in agreement with the value derived from the surface brightness photometry of the H α emission.
- The sphere is partially filled (filling factor $\simeq 0.1$) with ionized gas that is very tenuous, having electron density of $\simeq 30 \text{ cm}^{-3}$.
- [O I]6300 and [O III]4363 emissions are well accounted for by photoionization.

Particular results from the modelling of the ultraviolet continuum are:

- The extinction affecting the stellar cluster is little, $E(B - V) = 0.1$, if the LMC extinction law is used to derive the value, or $E(B - V) = 0.2$ if the Calzetti et al. (1994) extinction law is used. The 3 Myr instantaneous burst spectral energy distribution is well matched by the spectrum of NGC 604 corrected with any of these two extinction laws. The value of the extinction is similar to the average extinction, $A_V = 0.5$, derived for the gas by Churchwell & Goss (1999).
- The massive cluster provides a number of high energy photons that is enough to photoionize the whole nebula. Thus, within the limits of the integrated models that we develop for a uniform geometry, our results are compatible with most of the ionizing radiation being reprocessed in the nebula, with no significant escape of ionizing photons.
- The wind power provided by the massive stars of the cluster is enough to form the central hole structure where the core stellar cluster is located. However, it cannot provide all the wind power required for the formation of the (at least) five shell structures seen in the H α image.
- The number of massive stars estimated is in agreement

with that derived from photometric studies based on the detection of individual stars.

ACKNOWLEDGMENTS

It is a pleasure to thank Gary Ferland and Claus Leitherer for kindly making their codes available, and Jaime Perea for the use of SIPL. Claus suggested that something should be done with those *IUE* spectra. We have benefited from stimulating and helpful discussions with members of the GEFÉ collaboration, in particular with Angeles Díaz, Jesús Maíz-Apellániz, Divakara Mayya, Guillermo Tenorio-Tagle, Elena Terlevich, Roberto Terlevich and José M. Vílchez. We are also indebted to Grazyna Stasińska for his detailed comments from a thorough reading of the paper. The *IUE* helpdesk have always been solicitous with our queries, in particular we acknowledge Pedro Rodríguez Pascual and Rosario González Riestra for support with the *IUE* spectra. *HST* images were retrieved from the ST-ECF *HST* archive.

REFERENCES

- Calzetti D., Kinney A.L., Storchi-Bergmann T., 1994, *ApJ*, 429, 582
- Cassatella A., Altamore A., González-Riestra R., Ponz J.D., Barbero J., Talavera A., Wamsteker W., 2000, *A&AS*, 141, 331
- Charbonnel C., Meynet G., Maeder A., Schaller G., Schaerer D., 1993, *A&AS*, 101, 415.
- Churchwell E., Goss W.M., 1999, *ApJ*, 514, 188
- Cid Fernandes R., Dottori H.A., Gruenwald R.B., Viegas S.M., 1992, *MNRAS*, 255, 165
- Conti P.S., Massey P., 1981, *ApJ*, 249, 471
- Clayton C.A., 1988, *MNRAS*, 231, 191
- D'Odorico S., Dopita M.A., Benvenuti P., 1980, *A&AS*, 40, 67
- D'Odorico S., Rosa M., 1981, *ApJ*, 248, 1015
- Díaz A.I., Terlevich E., Pagel B.E.J., Vílchez J.M., Edmunds M.G., 1987, *MNRAS*, 226, 19
- Drissen L., Moffat A.F.J., Shara M.M., 1990, *ApJ*, 364, 496
- , 1993, *AJ*, 105, 1400
- , Roy J.-R., Robert C., Devost D., Doyon R. 2000, *AJ*, 119, 688
- Ferland G.J., 1997, *Hazy*, a Brief Introduction to CLOUDY, University of Kentucky, Department of Physics and Astronomy Internal Report
- Freedman W.L., Wilson C.D., Madore B.F., 1991, *ApJ*, 372, 455
- García-Vargas M.L., Díaz A.I., 1994, *ApJS*, 91, 553
- , Bressan A., Díaz A.I., 1995a, *A&AS*, 112, 13
- , Bressan A., Díaz A.I., 1995b, *A&AS*, 112, 35
- , González-Delgado R.M., Pérez E., Alloin D., Díaz A.I., Terlevich E., 1997, *ApJ*, 478, 112
- González Delgado R.M., Heckman T., Leitherer C., Meurer G., Krolik J., Wilson A.S., Kinney A.L., Koratkar A., 1998, *ApJ*, 505, 174
- , García-Vargas M.L., Goldader J., Leitherer C., Pasquali A., 1999a, *ApJ*, 513, 707
- , Leitherer C., 1999, *ApJS*, 125, 479
- , Leitherer C., Heckman T., 1999b, *ApJS*, 125, 489
- González-Riestra R., Cassatella A., Solano E., Altamore A., Wamsteker W. 2000, *A&AS*, 141, 343
- Hawley S.A., Grandi S.A., 1977, *ApJ*, 217, 420
- Hippenlein H., Fried J.W., 1984, *A&A*, 141, 49
- Hunter D.A., Baum W.A., O'Neil E.J., Lynds R., 1996, *ApJ*, 456, 174
- Israel F.P., van der Kruit P.C., 1974, *A&A*, 32, 363
- Kennicutt R.C., 1984, *ApJ*, 287, 116
- Kobulnicky H.A., Zaritsky D., 1999, *ApJ*, 511, 120
- Kwitter K.B., Aller L.H., 1981, *MNRAS*, 195, 939
- Leitherer C., 1997, in Waller W.H., Fanelli M.N., Hollis J.E., Danks A.C., eds., *AIP Conf. Procs.* 408, American Institute of Physics, New York, p. 119
- Leitherer C., Heckman T.M., 1995, *ApJS*, 96, 9
- , Robert C., Drissen L. 1992, *ApJ*, 401, 596
- , Robert C., Heckman T.M., 1995, *ApJS*, 99, 173
- , Schaerer D., Goldader J.D., González Delgado R.M., Robert C., Foo Kune D., de Mello D.F., Devost D., Heckman T.M., 1999, *ApJS*, 123, 3
- , Vacca W.D., Conti P.S., Filippenko A.V., Robert C., Sargent W.L.W., 1996, *ApJ*, 465, 717
- Lejeune T., Buser R., Cuisinier F., 1997, *A&AS*, 125, 229
- Luridiana V., Peimbert M., Leitherer C., 1999, *ApJ*, 527, 110
- Madau P., Ferguson H.C., Dickinson M.E., Giavalisco M., Steidel C.C., Fruchter A., 1996, *MNRAS*, 283, 1388
- Maíz-Apellániz, J., 1999, PhD Thesis, Univ. Complutense de Madrid
- Mas-Hesse J.M., Kunth D., 1999, *A&A*, 349, 765
- Massey P., Hutchings J.B., 1983, 275, 578
- McClure R.D., Racine R., 1969, *AJ*, 74, 1000
- Medina Tanco G.A., Sabalisk N., Jatenco-Pereira V., Opher R., 1997, *ApJ*, 487, 163
- Meynet G., Maeder A., Schaller G., Schaerer D., Charbonnel C., 1994, *A&AS*, 103, 97
- Morton D.C., 1967, *ApJ*, 147, 1017
- Muñoz-Tuñón C., Tenorio Tagle G., Castañeda H.O., Terlevich R., 1996, *AJ*, 112, 1636
- Peimbert M., 1970, *PASP*, 82, 636
- Robert C., Leitherer C., Heckman T.M., 1993, *ApJ*, 418, 749
- Rodríguez-Pascual P.M., González-Riestra R., Schartel N., Wamsteker W. 1999, *A&AS*, 139, 183
- Rosa M., D'Odorico S., 1982, *A&A*, 108, 339
- Rosa M., Joubert M., Benvenuti P., 1984, *A&AS*, 57, 361
- Rosa M., Solf J., 1984, *A&A*, 130, 29
- Sabalisk N.S.P., Tenorio-Tagle G., Castañeda H.O., Muñoz-Tuñón C., 1995, *ApJ*, 444, 200
- Schaerer D., Charbonnel C., Meynet G., Maeder A., Schaller G., 1993a, *A&AS*, 102, 339
- Schaerer D., Meynet G., Maeder A., Schaller G., 1993b, *A&AS*, 98, 523
- Schaller G., Schaerer D., Meynet G., Maeder A., 1992, *A&AS*, 96, 269
- Schmutz W., Leitherer C., Gruenwald R.B., 1992, *PASP*, 104, 1164
- Smith H.E., 1975, *ApJ*, 199, 591
- Stasińska G., Leitherer C., 1996, *ApJS*, 107, 661
- Stasińska G., Schaerer D., 1999, *A&A*, 351, 72
- Terlevich E., Díaz A.I., Terlevich R., González Delgado R.M., Pérez E., García-Vargas M.L., 1996, *MNRAS*, 279, 1219
- Vacca W.D., Robert C., Leitherer C., Conti P.S., 1995, *ApJ*, 444, 647
- Viallefond F., Goss W.M., 1986, *A&A*, 154, 357
- Vílchez J.M., Pagel B.E.J., 1988, *MNRAS*, 231, 257
- Walborn N.R., 1991, in Leitherer C., Walborn N., Heckman T., Norman C., eds, *Massive Stars in Starbursts*. Cambridge Univ. Press, Cambridge, p. 145
- Walborn N.R., Fitzpatrick E. L., 1990, *PASP*, 102, 379
- Yang H., Chu Y.-H., Skillman E.D., Terlevich R., 1996, *AJ*, 112, 146

This figure "fig1.jpg" is available in "jpg" format from:

<http://arxiv.org/ps/astro-ph/0003067v1>

This figure "fig2.jpg" is available in "jpg" format from:

<http://arxiv.org/ps/astro-ph/0003067v1>